Synthesizing Five-Body Interaction in a Superconducting Quantum Circuit

Ke Zhang,[1,*] Hekang Li,[1,*] Pengfei Zhang,[1] Jiale Yuan,[1] Jinyan Chen,[1] Wenhui Ren,[1] Zhen Wang,[1] Chao Song[1,†],
Da-Wei Wang,[1,3,‡] H. Wang,[1,2] Shiyao Zhu,[1,2] Girish S. Agarwal,[4] and Marlan O. Scully[4,§]

[1]*Interdisciplinary Center for Quantum Information, State Key Laboratory of Modern Optical Instrumentation, and
Zhejiang Province Key Laboratory of Quantum Technology and Device, Department of Physics,
Zhejiang University, Hangzhou 310027, China*
[2]*Hangzhou Global Scientific and Technological Innovation Center, Zhejiang University, Hangzhou 311215, China*
[3]*CAS Center of Excellence in Topological Quantum Computation, Beijing 100190, China*
[4]*Institute of Quantum Science and Engineering, Texas A&M University, College Station, Texas 77843, USA*

Synthesizing many-body interaction Hamiltonians is a central task in quantum simulation. However, it is challenging to synthesize Hamiltonians that have more than two spins in a single term. Here we synthesize m-body spin-exchange Hamiltonians with m up to 5 in a superconducting quantum circuit by simultaneously exciting multiple independent qubits with time-energy correlated photons generated from a qudit. The dynamic evolution of the m-body interaction is governed by the Rabi oscillation between two m-spin states, in which the states of each spin are different. We demonstrate the scalability of our approach by comparing the influence of noises on the three-, four- and five-body interaction and building a many-body Mach-Zehnder interferometer which potentially has a Heisenberg-limit sensitivity. This study paves a way for quantum simulation involving many-body interaction Hamiltonians such as lattice gauge theories in quantum circuits.

The synthesis of many-body interaction Hamiltonians plays a vital role in quantum simulation and quantum computing. Most quantum gates [1] rely on two-body interactions, based on which state-of-the-art quantum circuits have been built [2–4], and quantum supremacy has been claimed [2,4]. Although these quantum circuits contain tens of qubits, each term of the Hamiltonian involves no more than two spin operators. To exploit the full degree of freedom in simulating emergent many-body physics with superconducting circuits, we need to synthesize arbitrary interaction among a large number of qubits [5–8]. In particular, for the current stage of quantum simulation in noisy intermediate-scale quantum circuits, fermionic Hamiltonians are typically mapped into multi-spin interaction Hamiltonians via a Jordan-Wigner transformation [9]. To meet this challenge the antisymmetric spin-exchange interaction [10,11] has been synthesized by breaking the time-reversal symmetry through Floquet modulation [12]. Similar techniques have been applied to the synthesis of effective gauge field [13] and a three-spin chirality Hamiltonian [14], which is a necessary element in simulating chiral spin liquid [15] and promising to realize the topological states of quantized light [16–18]. Up to now the largest number of spin operators in a single term of the Hamiltonian was achieved in the four-spin ring-exchange interaction of cold atoms in optical lattices [19], and in the four-spin phase gate in superconducting circuits [20,21].

While the direct capacitive or inductive coupling between superconducting qubits [22–24] is limited to two-body interaction [25], many methods have been proposed [26–32] to synthesize many-body interaction Hamiltonians in superconducting circuits. In particular, higher excited states in superconducting circuits can be used to synthesize interactions involving more than 2 qubits [33–35]. Nevertheless, interaction Hamiltonians involving many spin operators, which are necessary ingredients for simulating lattice gauge theories [36–39] and topological quantum computing [40], have been difficult to be realized in superconducting qubits. Here we report the synthesis of m-body (with m up to 5) spin-exchange interaction Hamiltonian with time-frequency correlated photons [41] in a superconducting quantum circuit, which breaks the record of the number of qubits in a single term of interaction Hamiltonians thus far synthesized on artificial quantum platforms. The interaction strength is large enough for collective coherence to be observed, allowing for a one-step generation of genuinely entangled five-spin Greenberger-Horne-Zeilinger (GHZ) states. We also use such multispin interaction to build nonlinear interferometers and simulate the effect of noises in the quantum tunneling between left- and right-handed molecules.

Five-body interaction in a superconducting circuit.— The experiment is performed in a superconducting circuit where four transmon qubits are symmetrically coupled to a central transmon qudit [see Fig. 1(a)]. All of the five
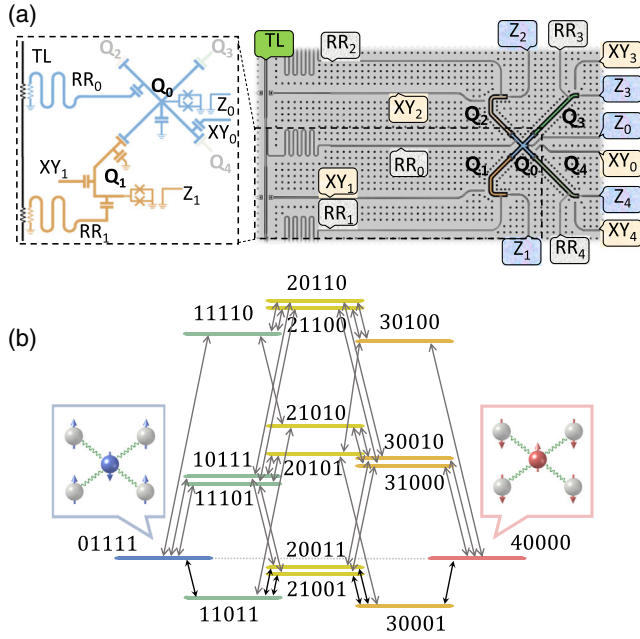
FIG. 1. (a) Device schematic and image illustrating the five frequency-tunable transmon circuits labeled from Q_0 to Q_4, with Q_0 being surrounded by Q_1 to Q_4. Each circuit Q_j has its own flux bias line Z_j for fast frequency tuning, microwave line XY_j for SU(2) spin rotation, and readout resonator RR_j that couples to a common transmission line TL for dispersive readout of Q_j's state. The dots in the image are bumps for the flip-chip process. Inset: the structure of the circuits in the dashed line area including Q_0 and Q_1. (b) Energy configurations of the qudit and four qubits for the five-body interaction. The lines denote the levels with distances in a vertical direction proportional to their energy differences. The double arrows denote the allowed transitions with the black ones denoting the major contributing paths.

transmon circuits have a sinusoidal potential well that hosts multiple energy levels [42]. The four surrounding qubits Q_j with $j = 1$–4 are used as two-level artificial atoms, while the central qudit Q_0 plays the role of a five-level atom, which generates cascade time-energy correlated photon quadruples. The transition frequencies between the ground state $|0\rangle$ and the first excited state $|1\rangle$ of the transmon circuits are tunable from 4 to 6 GHz. The coupling strengths $g_j/2\pi$ between the surrounding qubits Q_j and the central qudit Q_0 are around 23 MHz, while those between the surrounding qubits are smaller than 1 MHz. The Hamiltonian of the system in the rotating-wave approximation is given by (we set $\hbar = 1$),

$$H = \sum_{n=1}^{4}\sum_{k=1}^{n} \nu_k |n_0\rangle\langle n_0| + \sum_{j=1}^{4} \omega_j |1_j\rangle\langle 1_j|$$
$$+ \sum_{n=1}^{4}\sum_{j=1}^{4} \sqrt{n}\, g_j(S_n^+\sigma_j^- + \sigma_j^+ S_n^-), \quad (1)$$

where $|n_j\rangle$ is the nth ($n = 0, 1, 2, \ldots$) level of Q_j, $S_n^+ \equiv |n_0\rangle\langle(n-1)_0|$ are the raising operators between the adjacent levels of Q_0, $\sigma_j^+ \equiv |1_j\rangle\langle 0_j|$ are the raising operators of the qubit Q_j with S_n^- and σ^- being their lowering operators, ν_k is the kth transition frequency between the energy levels $|k_0\rangle$ and $|(k-1)_0\rangle$ of the qudit Q_0, and ω_j is the transition frequency of the qubit Q_j. The factor $\sqrt{n}$ in the coupling strengths between Q_0 and other qubits is due to the bosonic nature of the mode in the transmon circuit, i.e., $\sqrt{n}S_n^-$ is equivalent to the matrix element of the annihilation operator between the Fock states $|n\rangle$ and $|n-1\rangle$.

The five-body spin-exchange interaction Hamiltonian is realized when we arrange the transition frequencies of all qubits to satisfy the four-photon resonance, $\sum_{k=1}^{4}\nu_k = \sum_{j=1}^{4}\omega_j$, while the single photon, two-photon, and three-photon resonances are avoided [see Fig. 1(b)]. The time-frequency correlated photon source, i.e., the qudit, plays a vital role in achieving such multibody interaction. The key element in our approach is that the qudit emits four photons sequentially with different frequencies: ν_4, ν_3, ν_2, and ν_1. The resulted effective Hamiltonian is

$$H_{\mathrm{eff}} = \lambda \Xi_4^- \sigma_1^+ \sigma_2^+ \sigma_3^+ \sigma_4^+ + \mathrm{H.c.}, \quad (2)$$

where $\Xi_n^- \equiv |0_0\rangle\langle n_0|$ is the lowering operator of the qudit from the nth excited state to the ground state, and λ is the fourth order effective coupling strength. If we replace the qudit with a resonator, i.e., in the traditional central cavity configuration [43–45], the qubits cannot be simultaneously excited, because all possible quantum paths cancel out, and we obtain $\lambda = 0$ (see Supplemental Material [46]).

Dynamic evolution and the GHZ state.—The controlling sequence diagram for the dynamics of H_{eff} is sketched in Fig. 2(a). We prepare the qubits in the initial state $|\Psi(0)\rangle = |01111\rangle$ at their idle frequencies. Then the 4 qubits are quickly biased to their interaction frequencies ω_j. After an interaction time τ, we bring the qubits to their readout frequencies for measurement (see the Supplemental Material [46] for values of transition frequencies for qubit initialization and readout). The results of the joint measurement of the wave function $|\Psi(\tau)\rangle = c_1(\tau)|01111\rangle + c_2(\tau)|40000\rangle$, ignoring the insignificant terms, are shown in Fig. 2(b), where the experimentally obtained probabilities of $|c_1(\tau)|^2$ and $|c_2(\tau)|^2$ (colored dots with error bars) are plotted in comparison with the numerical simulation (colored lines) obtained from the original Hamiltonian in Eq. (1). The Rabi oscillation between the two states is observed as expected. In the numerical simulation, we use the quantum master equation with the experimentally measured energy relaxation time $T_{1,j}$ and the empirical pure dephasing time $T_{\varphi,j}$ ($\approx 6T_{2,j}^*$ where $T_{2,j}^*$ is the experimentally measured Ramsey Gaussian dephasing time) to capture the impact of decoherence [45,46,54].
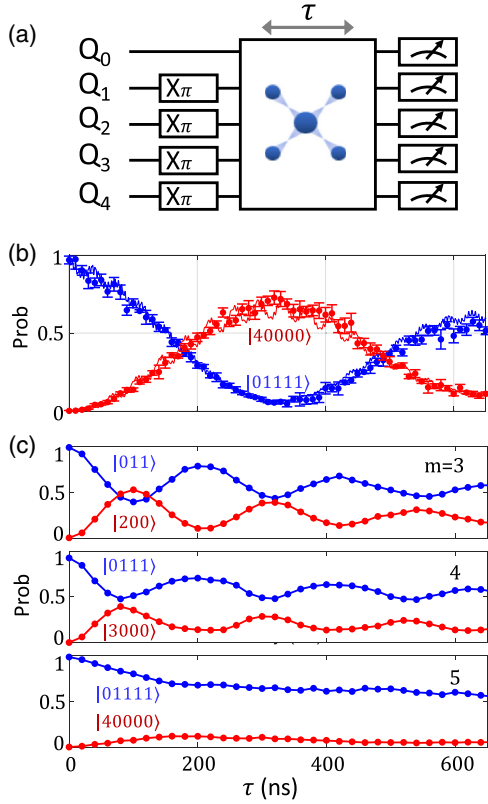
FIG. 2. (a) Sequence diagram for observing the dynamic evolution. After preparing the system to the initial state $|01111\rangle$ by applying X_π rotation (a π rotation around x axis) to Q_j with $j = 1$–4, we quickly tune the transition frequencies of all qubits to activate the five-body interaction. After a specific time τ, the occupational probabilities of the system for different computational states are measured. (b) The experimentally measured occupational probabilities of $|c_1(\tau)|^2$ for $|01111\rangle$ (blue dots) and $|c_2(\tau)|^2$ for $|40000\rangle$ (red dots) for different interaction times τ. Error bars represent statistical errors. Lines are the results obtained by numerical simulation, where five and three levels are considered for Q_0 and other qubits, respectively. (c) The effect of noises on the evolution under the m-body spin-exchange Hamiltonian. The low-frequency noises are simulated by random detunings between the two states in the interaction. Except for the added noises, the sequence diagrams are similar to the one in (a) but for different m's. The populations of the two relevant states are measured as functions of time. The noises have a destructive effect on the coherent tunneling between the two spin configurations, which is demonstrated by the diminishing oscillation contrast when we increase m from 3 to 5.

The Rabi oscillation period of the five-body spin-exchange interaction is estimated to be about 0.6 μs, which is short compared with the decoherence time and allows the generation of a five-spin GHZ state in a single step. At $\tau = 170$ ns, the state evolves to $|\Psi\rangle = (|01111\rangle + e^{i\phi}|40000\rangle)/\sqrt{2}$ with ϕ being a trivial dynamical phase. The measured fidelity, which is defined as $F = \mathrm{Tr}(\rho_{\mathrm{ideal}} \cdot \rho_{\mathrm{exp}})$ with ρ_{ideal} and ρ_{exp} being the ideal and experimental density matrices, is estimated to be

0.685 ± 0.022 by directly measuring the four nonzero elements of the density matrix from the many-body interference, which is consistent with the lower bound obtained by quantum state tomography [46] and satisfies the criterion of global entanglement. Based on the numerical simulations, we attribute an intrinsic error of around 0.057 to interactions other than the five-body interaction, and an error of around 0.087 to the decoherence effects. The additional interaction inserted in detecting the off-diagonal terms contributes to an error of around 0.107. The remaining error of around 0.064 may come from the imperfect control pulses.

In the traditional approach of GHZ state generation [55–58], the effective Hamiltonian only contains two-body terms, and all states in the symmetric subspace are involved, forbidding a two-state Rabi oscillation, while in our approach only the two relevant states are involved, such that we can simulate the quantum tunneling between the left- and right-handed molecules.

Simulating decoherence effect in the tunneling between two chiral molecules.—Since the early days of quantum mechanics, the origin of chiral molecules has puzzled generations of physicists [59–64]. In particular, Hund argued that the parity operator commutes with the electromagnetic interaction Hamiltonian, such that stable molecular states shall conserve parity, which is contradictory to the existence of chiral molecules [59]. To resolve the paradox, an argument is that the left- and right-handed molecules reside in two energy valleys, and the tunneling strength between them is so small that it takes a macroscopically long time for large chiral molecules to tunnel from one configuration to the other. During this process environmental noises induce decoherence and hinder the tunneling, which is similar to the quantum Zeno effect [63]. The two quantum states involved in the five-body interaction can be used to simulate the tunneling between the left- and right-handed molecular states, such that the effect of environmental noises can be investigated toward the question of the stabilization of chiral molecules. We need to emphasize that while two chiral molecules are mirror symmetric to each other, the two states $|40000\rangle$ and $|01111\rangle$ in our simulation are time-reversal symmetric to each other. The electromagnetic interaction between atoms in the chiral molecules preserves the parity symmetry while the five-body interaction Hamiltonian preserves the time-reversal symmetry. Since the argument in the Hund paradox is still valid by replacing parity symmetry with time-reversal symmetry, we are simulating the quantum tunneling between two chiral molecules with the one between two time-reversal symmetric spin configurations, but not the chirality itself.

As a step in this direction, in Fig. 2(c) we simulate the suppressed tunneling between two chiral molecules due to slow environmental noises, which can also be considered as a random potential difference between the two chiral molecules. To demonstrate this, we artificially inject

arbitrary flux noises to the system during the five-body interaction. Each circuit Q_j is offset from its interaction frequency by a small amount of $\delta_{j,k}$, which is randomly chosen in a range of $[-\Delta_j, \Delta_j]$ but fixed for the kth pulse sequence. In the experiment, the noise strength $\Delta_0/2\pi \approx 5$ MHz for Q_0 between the transition from the state $|0_0\rangle$ to $|4_0\rangle$. The noise range $\Delta_j/2\pi$ is set to be about 5 MHz for all other qubits Q_j. An ensemble of 20 pulse sequences is applied to emulate the random white noise that shifts the energy of Q_j. It has been shown that this is an efficient way to simulate artificial dephasing [65] and many-body localization [54,66]. For each sequence, we record the probabilities of the two states as a function of time. We average over 20 traces and find that the oscillation between the two states vanishes, as shown in Fig. 2(c). By exciting Q_0 to the second or third excited state and coupling it to 2 or 3 qubits, we synthesize the three- or four-body spin-exchange Hamiltonians, $\lambda_3 \Xi_2^- \sigma_1^+ \sigma_2^+ + \text{H.c.}$ or $\lambda_4 \Xi_3^- \sigma_1^+ \sigma_2^+ \sigma_3^+ + \text{H.c.}$, where $\lambda_3/2\pi \approx 2.25$ MHz and $\lambda_4/2\pi \approx 2.29$ MHz are the interaction strengths obtained from the Rabi periods (see the Supplemental Material [46] for parameters of the circuits). The same noise strength has a smaller effect on the four- and three-body interaction, resulting from a larger interaction strength and a weaker noise-induced decoherence effect. The oscillation between the two states is still visible, although partially smeared by the noises.

Many-body interferometer.—The many-body spin-exchange Hamiltonian can be used to build a Mach-Zehnder interferometer that has a Heisenberg-limit sensitivity [67]. In the m-body interferometer, we introduce an energy-splitting Hamiltonian $B_z(\sum_{j=1}^{m-1} \sigma_j^z - \Xi_{m-1}^z)$ where $\Xi_m^z \equiv |m_0\rangle\langle m_0| - |0_0\rangle\langle 0_0|$ and B_z is an artificial magnetic field. The dynamic phase induced by this Hamiltonian can be detected as follows. We first prepare the state $|0\rangle \otimes |1\rangle^{\otimes(m-1)}$ and then activate the m-body interaction for a fixed time $\tau_I \sim 2\pi/8\lambda_m$ to steer the system to the GHZ state. In the experiment, τ_I is slightly adjusted for an optimized GHZ state fidelity and set to be 60 ns (55 ns, 170 ns) for $m = 3$ (4, 5). Then we apply local magnetic fields on each spin-1/2 particle, which is synthesized by applying a square Z pulse to each transmon circuit for a specific time τ_B and with a strength of $-\Delta_B$ (between states $|0\rangle$ and $|m-1\rangle$) for Q_0 and Δ_B for other qubits. $\Delta_B/2\pi$ is fixed to be around 5 MHz in the experiment. After activating the m-body interaction again for a time τ_I, we measure the occupational probabilities of $|c_1(\tau_B)|^2$ for $|0\rangle \otimes |1\rangle^{\otimes(m-1)}$ and $|c_2(\tau_B)|^2$ for $|m-1\rangle \otimes |0\rangle^{\otimes(m-1)}$. The controlling sequence for a five-body interferometer is shown in Fig 3(a). The oscillation frequency scales linearly with m, as shown by the data in Fig. 3(b). Although the sensitivity is not enhanced to the Heisenberg limit due to a lowered visibility of the oscillation for larger m, we note that the oscillation amplitude infers the off diagonal term ρ_{off} of the GHZ state by $|c_1(\tau_B)|^2 = -|\rho_{\text{off}}| \cos(2\pi m \Delta_B \tau_B) + \text{const}$, which dramatically reduces the number of quantum operations required to benchmark the GHZ state fidelity compared with the traditional tomography method. We note that the
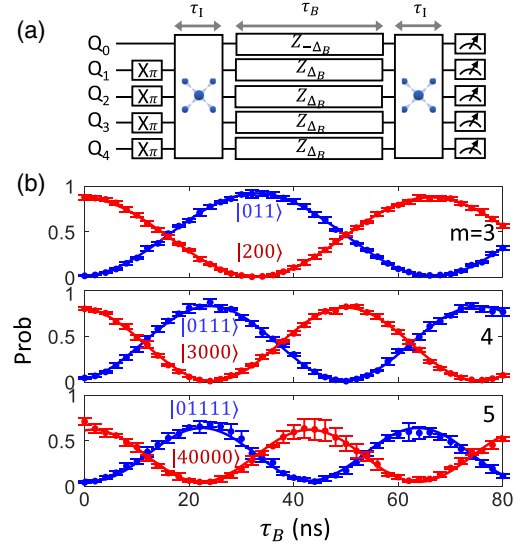
FIG. 3. (a) Sequence diagram for detecting the magnetic field leveraging the m-body interaction, with $m = 5$ here as an example. The magnetic field is synthesized by applying to each transmon circuit a square Z pulse to offset its transition frequency between states $|0\rangle$ and $|m-1\rangle$ ($|1\rangle$) for Q_0 (other qubits) by an amount of $-\Delta_B$ (Δ_B) for a time τ_B. The dynamical phase accumulated during this process can be detected by sandwiching itself between two m-body interaction operations with a fixed time $\tau_I \sim 2\pi/8\lambda_m$. (b) The experimentally measured occupational probabilities of $|c_1(\tau_B)|^2$ (blue dots) and $|c_2(\tau_B)|^2$ (red dots) for different time τ_B. Lines are the fitting results. The fitted oscillation frequencies for $m = 3$, 4, 5 are 14.9, 19.5, and 24.2 MHz respectively, agreeing well with the ratio of $3:4:5$.

GHZ state obtained from the all-to-all spin interaction can also be used to build a Heisenberg-limit interferometer [68,69]. However, in that case all states in the symmetric subspace are involved, and the approach is more prone to noises compared with the current approach, which only involves two states.

Conclusion.—We experimentally realize m-body spin-exchange interaction Hamiltonians with m up to 5, which can still be increased to larger numbers in upgraded circuits with larger coupling strengths and lower decoherence rates. It is ready to be implemented in quantum circuits of tens of qubits [70,71], such as in a square lattice where qubits interact with their four neighbors with the five-body Hamiltonian H_{eff}, in simulating the lattice gauge theory or Jordan-Wigner transformed fermionic Hamiltonians. The essential difference between our approach and existing methods in coupling multiple spins is that we have $m > 2$ spins in one term of the Hamiltonian. Such uniqueness enables us to simulate the quantum tunneling between chiral molecules and build a many-body interferometer.

---

[*]K. Z. and H. L. contributed equally to this work.
[†]chaosong@zju.edu.cn
[‡]dwwang@zju.edu.cn
[§]scully@tamu.edu

[1] A. Barenco, C. H. Bennett, R. Cleve, D. P. DiVincenzo, N. Margolus, P. Shor, T. Sleator, J. A. Smolin, and H. Weinfurter, Elementary gates for quantum computation, Phys. Rev. A **52**, 3457 (1995).

[2] F. Arute *et al.*, Quantum supremacy using a programmable superconducting processor, Nature (London) **574**, 505 (2019).

[3] P. Jurcevic *et al.*, Demonstration of quantum volume 64 on a superconducting quantum computing system, arXiv:2008.08571.

[4] Y. Wu *et al.*, Strong Quantum Computational Advantage using a Superconducting Quantum Processor, Phys. Rev. Lett. **127**, 180501 (2021).

[5] R. Babbush, N. Wiebe, J. McClean, J. McClain, H. Neven, and GarnetKin-Lic Chan, Low-Depth Quantum Simulation of Materials, Phys. Rev. X **8**, 011044 (2018).

[6] K. Bharti *et al.*, Noisy intermediate-scale quantum (NISQ) algorithms, Rev. Mod. Phys. **94**, 015004 (2022).

[7] X. Peng, J. Zhang, J. Du, and D. Suter, Quantum Simulation of a System with Competing Two- and Three-Body Interactions, Phys. Rev. Lett. **103**, 140501 (2009).

[8] I. M. Georgescu, S. Ashhab, and F. Nori, Quantum simulation, Rev. Mod. Phys. **86**, 153 (2014).

[9] S. McArdle, S. Endo, A. Aspuru-Guzik, S. C. Benjamin, and X. Yuan, Quantum computational chemistry, Rev. Mod. Phys. **92**, 015003 (2020).

[10] I. E. Dzialoshinskii, Thermodynamic theory of weak ferromagnetism in antiferromagnetic substances, J. Exp. Theor. Phys. **32**, 1547 (1957).

[11] T. Moriya, New Mechanism of Anisotropic Superexchange Interaction, Phys. Rev. Lett. **4**, 228 (1960).

[12] D. W. Wang *et al.*, Synthesis of antisymmetric spin exchange interaction and chiral spin clusters in superconducting circuits, Nat. Phys. **15**, 382 (2019).

[13] P. Roushan *et al.*, Chiral ground-state currents of interacting photons in a synthetic magnetic field, Nat. Phys. **13**, 146 (2017).

[14] W. Liu, W. Feng, W. Ren, D. W. Wang, and H. Wang, Synthesizing three-body interaction of spin chirality with superconducting qubits, Appl. Phys. Lett. **116**, 114001 (2020).

[15] X. G. Wen, F. Wilczek, and A. Zee, Chiral spin states and superconductivity, Phys. Rev. B **39**, 11413 (1989).

[16] H. Cai and D. W. Wang, Topological phases of quantized light, Natl. Sci. Rev. **8**, nwaa196 (2021).

[17] J. Yuan, H. Cai, C. Wu, S. Y. Zhu, R. B. Liu, and D. W. Wang, Unification of valley and anomalous hall effects in a strained lattice, Phys. Rev. B **104**, 035410 (2021).

[18] D. Cheng, B. Peng, D. W. Wang, X. Chen, L. Yuan, and S. Fan, Arbitrary synthetic dimensions via multiboson dynamics on a one-dimensional lattice, Phys. Rev. Research **3**, 033069 (2021).

[19] H. N. Dai, B. Yang, A. Reingruber, H. Sun, X.-F. Xu, Y.-A. Chen, Z.-S. Yuan, and J.-W. Pan, Four-body ring-exchange interactions and anyonic statistics within a minimal toric-code hamiltonian, Nat. Phys. **13**, 1195 (2017).

[20] H. Paik *et al.*, Experimental Demonstration of a Resonator-Induced Phase Gate in a Multiqubit Circuit-QED System, Phys. Rev. Lett. **117**, 250502 (2016).

[21] C. Song *et al.*, Continuous-variable geometric phase and its manipulation for quantum computation in a superconducting circuit, Nat. Commun. **8**, 1061 (2017).

[22] J. Q. You and F. Nori, Atomic physics and quantum optics using superconducting circuits, Nature (London) **474**, 589 (2011).

[23] M. H. Devoret and R. J. Schoelkopf, Superconducting circuits for quantum information: An outlook, Science **339**, 1169 (2013).

[24] M. Kjaergaard, M. E. Schwartz, J. Braumüller, P. Krantz, J. I.-J. Wang, S. Gustavsson, and W. D. Oliver, Superconducting qubits: Current state of play, Annu. Rev. Condens. Matter Phys. **11**, 369 (2020).

[25] P. Krantz, M. Kjaergaard, F. Yan, T. P. Orlando, S. Gustavsson, and W. D. Oliver, A quantum engineer's guide to superconducting qubits, Appl. Phys. Rev. **6**, 021318 (2019).

[26] L. Garziano, V. Macri, R. Stassi, O. DiStefano, F. Nori, and S. Savasta, One Photon can Simultaneously Excite Two or More Atoms, Phys. Rev. Lett. **117**, 043601 (2016).

[27] A. F. Kockum, A. Miranowicz, V. Macrì, S. Savasta, and F. Nori, Deterministic quantum nonlinear optics with single atoms and virtual photons, Phys. Rev. A **95**, 063849 (2017).

[28] P. Zhao, X. Tan, H. Yu, S. L. Zhu, and Y. Yu, Circuit QED with qutrits: Coupling three or more atoms via virtual-photon exchange, Phys. Rev. A **96**, 043833 (2017).

[29] R. Stassi, V. Macri, A. F. Kockum, O. DiStefano, A. Miranowicz, S. Savasta, and F. Nori, Quantum nonlinear optics without photons, Phys. Rev. A **96**, 023818 (2017).

[30] X. Liu, Q. Liao, G. Fang, and S. Liu, Dynamic generation of multi-qubit entanglement in the ultrastrong-coupling regime, Sci. Rep. **9**, 2919 (2019).

[31] C. Sánchez Muñoz, A. Frisk Kockum, A. Miranowicz, and F. Nori, Simulating ultrastrong-coupling processes breaking parity conservation in jaynes-cummings systems, Phys. Rev. A **102**, 033716 (2020).

[32] F. Petiziol, M. Sameti, S. Carretta, S. Wimberger, and F. Mintert, Quantum Simulation of Three-Body Interactions in Weakly Driven Quantum Systems, Phys. Rev. Lett. **126**, 250504 (2021).

[33] S. P. Pedersen, K. S. Christensen, and N. T. Zinner, Native three-body interaction in superconducting circuits, Phys. Rev. Research **1**, 033123 (2019).

[34] S. P. Pedersen and N. T. Zinner, Lattice gauge theory and dynamical quantum phase transitions using noisy intermediate-scale quantum devices, Phys. Rev. B **103**, 235103 (2021).

[35] W. Ren *et al.*, Simultaneous Excitation of Two Noninteracting Atoms with Time-Frequency Correlated Photon Pairs in a Superconducting Circuit, Phys. Rev. Lett. **125**, 133601 (2020).

[36] C. Schweizer, F. Grusdt, M. Berngruber, L. Barbiero, E. Demler, N. Goldman, I. Bloch, and M. Aidelsburger, Floquet approach to Z_2 lattice gauge theories with ultracold atoms in optical lattices, Nat. Phys. **15**, 1168 (2019).

[37] A. Mezzacapo, E. Rico, C. Sabin, I. L. Egusquiza, L. Lamata, and E. Solano, Non-Abelian SU(2) Lattice Gauge Theories in Superconducting Circuits, Phys. Rev. Lett. **115**, 240502 (2015).

[38] M. Müller, K. Hammerer, Y. L. Zhou, C. F. Roos, and P. Zoller, Simulating open quantum systems: From many-body interactions to stabilizer pumping, New J. Phys. **13**, 085007 (2011).

[39] E. Zohar, A. Farace, B. Reznik, and J. I. Cirac, Digital Quantum Simulation of Z_2 Lattice Gauge Theories with Dynamical Fermionic Matter, Phys. Rev. Lett. **118**, 070501 (2017).

[40] A. Kitaev, Fault-tolerant quantum computation by anyons, Ann. Phys. (Amsterdam) **303**, 2 (2003).

[41] A. Muthukrishnan, G. S. Agarwal, and M. O. Scully, Inducing Disallowed Two-Atom Transitions with Temporally Entangled Photons, Phys. Rev. Lett. **93**, 093002 (2004).

[42] L. Zhang, C. Song, H. Wang, and S. B. Zheng, Observation of geometric phase in a dispersively coupled resonator-qutrit system, Chin. Phys. B **27**, 070303 (2018).

[43] J. M. Fink, R. Bianchetti, M. Baur, M. Goppl, L. Steffen, S. Filipp, P. J. Leek, A. Blais, and A. Wallraff, Dressed Collective Qubit States and the Tavis-Cummings Model in Circuit QED, Phys. Rev. Lett. **103**, 083601 (2009).

[44] L. DiCarlo, M. D. Reed, L. Sun, B. R. Johnson, J. M. Chow, J. M. Gambetta, L. Frunzio, S. M. Girvin, M. H. Devoret, and R. J. Schoelkopf, Preparation and measurement of three-qubit entanglement in a superconducting circuit, Nature (London) **467**, 574 (2010).

[45] C. Song *et al.*, Generation of multicomponent atomic Schrödinger cat states of up to 20 qubits, Science **365**, 574 (2019).

[46] See Supplemental Material at http://link.aps.org/supplemental/10.1103/PhysRevLett.128.190502 for device characterization, controlling and measuring methods and detailed theoretical calculations, which contain Refs. [47–53].

[47] B. Foxen *et al.*, Qubit compatible superconducting interconnects, Quantum Sci. Technol. **3**, 014005 (2018).

[48] B. M. Niedzielski *et al.*, Silicon hard-stop spacers for 3D integration of superconducting qubits, arXiv:1907.12882.

[49] Y. Zheng, C. Song, M. C. Chen, B. Xia, W. Liu *et al.*, Solving Systems of Linear Equations with a Superconducting Quantum Processor, Phys. Rev. Lett. **118**, 210504 (2017).

[50] E. Magesan *et al.*, Efficient Measurement of Quantum Gate Error by Interleaved Randomized Benchmarking, Phys. Rev. Lett. **109**, 080505 (2012).

[51] K. Xu *et al.*, Emulating Many-Body Localization with a Superconducting Quantum Processor, Phys. Rev. Lett. **120**, 050507 (2018).

[52] H. Xu *et al.*, Coherent population transfer between uncoupled or weakly coupled states in ladder-type superconducting qutrits, Nat. Commun. **7**, 11018 (2016).

[53] C. Song, K. Xu, W. Liu, C. P. Yang, S. B. Zheng *et al.*, 10-Qubit Entanglement and Parallel Logic Operations with a Superconducting Circuit, Phys. Rev. Lett. **119**, 180511 (2017).

[54] Q. Guo *et al.*, Observation of energy-resolved many-body localization, Nat. Phys. **17**, 234 (2021).

[55] G. S. Agarwal, R. R. Puri, and R. P. Singh, Atomic Schrödinger cat states, Phys. Rev. A **56**, 2249 (1997).

[56] A. Sørensen and K. Mølmer, Entanglement and quantum computation with ions in thermal motion, Phys. Rev. A **62**, 022311 (2000).

[57] S. B. Zheng and G. C. Guo, Efficient Scheme for Two-Atom Entanglement and Quantum Information Processing in Cavity QED, Phys. Rev. Lett. **85**, 2392 (2000).

[58] A. Mezzacapo, L. Lamata, S. Filipp, and E. Solano, Many-Body Interactions with Tunable-Coupling Transmon Qubits, Phys. Rev. Lett. **113**, 050501 (2014).

[59] F. Hund, Zur Deutung der Molekelspektren. III., Z. Phys. **43**, 805 (1927).

[60] J. A. Cina and R. A. Harris, Superpositions of handed wave functions, Science **267**, 832 (1995).

[61] S. F. Mason, Origins of biomolecular handedness, Nature (London) **311**, 19 (1984).

[62] B. Darquié *et al.*, Progress toward a first observation of parity violation in chiral molecules by high-resolution laser spectroscopy, Chirality **22**, 870 (2010).

[63] J. Trost and K. Hornberger, Hund's Paradox and the Collisional Stabilization of Chiral Molecules, Phys. Rev. Lett. **103**, 023202 (2009).

[64] A. A. Houck, H. E. Türeci, and J. Koch, On-chip quantum simulation with superconducting circuits, Nature (London) **8**, 292 (2012).

[65] D. V. Averin, K. Xu, Y. P. Zhong, C. Song, H. Wang, and S. Han, Suppression of Dephasing by Qubit Motion in Superconducting Circuits, Phys. Rev. Lett. **116**, 010501 (2016).

[66] J. Smith, A. Lee, P. Richerme, B. Neyenhuis, P. W. Hess, P. Hauke, M. Heyl, D. A. Huse, and C. Monroe, Many-body localization in a quantum simulator with programmable random disorder, Nat. Phys. **12**, 907 (2016).

[67] P. Facchi, G. Florio, S. Pascazio, and F. V. Pepe, Greenberger-Horne-Zeilinger States and Few-Body Hamiltonians, Phys. Rev. Lett. **107**, 260502 (2011).

[68] G. S. Agarwal, *Quantum Optics* (Cambridge University Press, Cambridge, England, 2013).

[69] D. Leibfried *et al.*, Creation of a six-atom 'Schrödinger cat' state, Nature (London) **438**, 639 (2005).

[70] X. Zhang *et al.*, Observation of a symmetry-protected topological time crystal with superconducting qubits, arXiv:2109.05577.

[71] P. Zhang *et al.*, Probing quantum many-body scars on a superconducting processor, arXiv:2201.03438.